Enhanced relaxation of nanoparticle-bound supercoiled DNA in X-ray radiation†

Erika A. Foley, Joshua D. Carter, Fang Shan and Ting Guo*

Received (in Cambridge, UK) 9th March 2005, Accepted 26th April 2005
First published as an Advance Article on the web 24th May 2005
DOI: 10.1039/b503425f

A therapeutic methodology was developed based on the large X-ray absorption cross-section of gold nanoparticles at high photon energies (>81 keV). Experimental results showed that the amounts of the relaxed circular supercoiled DNA (scDNA) for gold nanoparticle-bound scDNA were more than doubled compared to that for free scDNA under otherwise identical radiation conditions.

Nanostructures have seen in an increasing number of applications in which fine-tuned properties of nanomaterials are discovered and employed. In the area of X-ray therapy, several novel methods have been reported. For example, directly injected gold nanoparticles have been used to treat cancer in mice.[1] Atomic nanogenerators and nanocomposites have also been developed.[2,3] In this report, potential applications of nanoparticles based on their X-ray photodynamic properties in X-ray radiation therapy are explored.

The cytotoxicity of ionizing radiation has been used for cancer treatment for decades.[4,5] A major source of toxicity is believed to originate from secondary species such as Auger electrons and radicals in aqueous solutions after X-ray absorption.[6] The Auger electrons can either interact with water molecules, a major constituent of the cell, to produce radicals that eventually react with and break the backbone of DNA or cleave base pairs from DNA;[7,8] or these electron can effectively cause single- and double-strand breaks (SSB and DSB) in DNA through direct interactions, as demonstrated using externally injected low-energy electrons.[9] It has been theoretically shown that these Auger electrons are effective within only 5–10 nm in physiological conditions.[10] Even with all these potentials, X-rays alone are an ineffective modality because they lack the selectivity toward killing only malignant cells.

We have developed a new method, which takes advantage of the large absorption cross-sections of high energy X-rays by nanoparticles of heavy elements. Because these nanoparticles can potentially be targeted to tumor sites via bioconjugation,[11–14] the combined specificity and cytotoxicity enabled by the necessity of the presence of *both* nanoparticles *and* delivery of radiation makes this method a potentially important therapeutic and diagnostic tool.

In our approach, gold nanoparticles were used to enhance X-ray absorption. Trimethylammonium (TMA) C_{12} functionalized gold nanoparticles (TMA_nAuNP, n denotes the number of TMA ligands on a nanoparticle) were synthesized (Electronic Supplementary Information†).[15–17] These positively charged ligands helped nanoparticles bind to DNA, which was supercoiled DNA (scDNA) (φX174, Form I, Invitrogen, Carlsbad, CA). When SSB occurred to scDNA, it became circular DNA (Form II), both appeared as a single band in gel electrophoresis. Experimental details are given in the ESI†.

Fig. 1 shows a TEM image of the TMA_nAuNP (left panel) and the size distribution (right panel). The average size of 5 nm was slightly larger than that made using the established procedure. Atomic force microscope (AFM) inspections showed a similar size distribution, peaked at 5 nm. These nanoparticles were used in all measurements described below.

Fig. 2 shows results of gel electrophoresis experiments designed to probe the interactions and mobility of scDNA and TMA_nAuNP. Details of the lane preparation are given in the ESI†. TMA_nAuNP were added into wells 2A, 3A, 5A, and 6A, and scDNA samples were added into wells 1A, 2A, 4B, 5B, and 6B. Wells 1B, 2B, 3B, and 4A were left empty.

Since TMA_nAuNP ($n \neq 0$) are positively charged and scDNA are negatively charged in 1 × TBE buffer, they moved in opposite directions in the gel, as shown in Fig. 2. TMA_nAuNP were visible as the stains spread to the right hand side of wells 2A, 3A, 5A, and 6A, indicating a distribution in the numbers of the TMA ligands on AuNP.

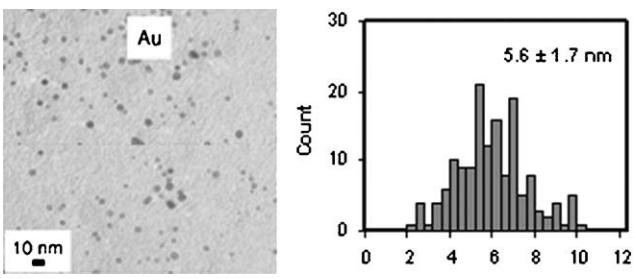

Fig. 1 Gold nanoparticles examined with TEM (left panel). The size distribution is shown in the right panel. The scale bar is 10 nm.

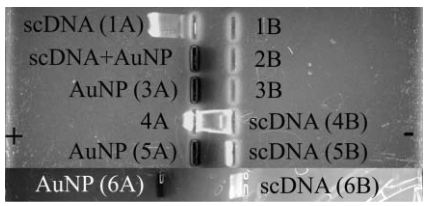

Fig. 2 Two agarose gels (0.8%) of TMAnAuNP and scDNA. The distances between the two columns of wells were different for lanes 1–5 and lane 6. Lanes are labelled as mA (left column) or mB, where m is the lane number 1 through 6. The polarity of the gels is shown with the + and − signs.

† Electronic supplementary information (ESI) available: experimental details. See http://www.rsc.org/suppdata/cc/b5/b503425f/

*tguo@ucdavis.edu

The migration of the scDNA in the wells of the right column in Fig. 2 was impeded by the presence of TMA_nAuNP travelling in the opposite direction in the same lanes. An example is given in lane 5, which shows that the scDNA was stopped well short of the normal distance travelled by the scDNA alone, as in lanes 1 and 4. In lane 6, the distance between the two wells was increased, and the scDNA travelled further than that in lane 5. An extreme case is shown in lane 2, in which the scDNA did not move out of the well 2A when it was mixed with TMA_nAuNP at a high nanoparticle-to-DNA ratio (~1000:1). In this case, the AuNP stain was still visible to the right of the well because of the large quantity used. The decreased mobility of the scDNA in the gel can be explained by the interactions of highly charged TMA_nAuNP with the scDNA.

Using the ratio of the distance traversed by the majority of TMA_nAuNP to that by the fastest moving TMA_nAuNP in lane 6, the upper limit of the number of TMA ligands on majority of the AuNP was estimated to be only 10% of the number of TMA ligands on the fastest moving AuNP. Assuming that there were 300 thiol ligands covering 900 surface Au atoms in a 5 nm nanoparticle, and with nearly 100 of those thiols being TMA ligands (the rest being dodecanethiol ligands), average AuNP had only ~10–15 TMA ligands on them.

Fig. 3 shows the gel electrophoresis results of radiation tests. scDNA and scDNA–TMA_nAuNP complexes were pipetted into the lanes of the gels. The lane assignments and running conditions are given in the ESI†. Fig. 3a shows the results of radiation tests, using samples of ~100:1 TMA_nAuNP-to-scDNA ratio. The scDNA occupied the spots further down the lanes, trailed by the relaxed scDNA.

After radiation, the amounts of the relaxed scDNA for scDNA–TMA_nAuNP mixtures increased. For example, both samples in lanes 3 and 9 in the inserts of Fig. 3a had the same radiation time of 2 minutes: In lane 9 almost half the scDNA were in the relaxed or circular form, whereas less than 25% of the scDNA were in this form in lane 3.

A lineout plot of the results of another gel is shown in Fig. 3b. The samples were prepared similarly to those used in Fig. 3a. As shown, there was little additional relaxation (~5%) caused by the presence of TMA_nAuNP (top panel in Fig. 3b). In contrast, the extent of the relaxation was almost the same for scDNA exposed for 4 min of radiation (dashed line) and for scDNA–TMA_nAuNP exposed for 2 min (solid line).

Three pairs of 6-set scDNA and 6-set scDNA–TMA_nAuNP samples were studied with radiation. Each pair of samples were identically prepared and irradiated, whereas the experimental conditions for different pairs varied slightly (ESI†). Fig. 4a shows the results of these radiation tests on the three pairs of free scDNA (empty symbols) and TMAAuNP-bound scDNA (corresponding solid symbols) samples. Depending on the experimental conditions, the percentage of the relaxed scDNA varied, although there were always more relaxed scDNA for radiated scDNA–TMA_nAuNP samples within each pair.

The maximum enhancement was observed between 0.5 and 2 Gy of radiation for the scDNA used here. The relative enhancement ratio, which is the ratio of the percentage of the relaxed DNA in the AuNP-bound scDNA to that of the relaxed DNA in free scDNA in each of the pair samples, is plotted in Fig. 4b. The ratios were calculated after corrections of relaxation prior to radiation.

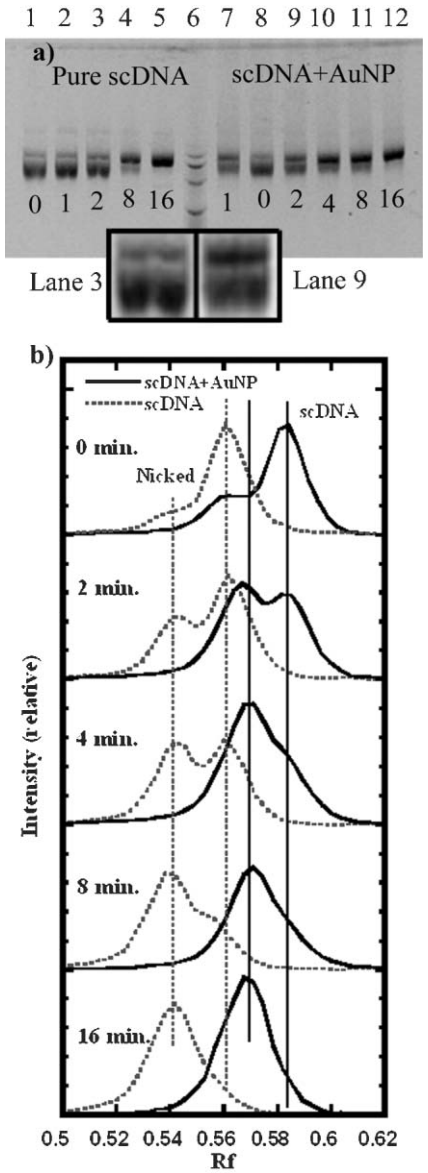

Fig. 3 (a) Results from the E-gels from the radiation testing. The lengths of the radiation (minutes) are shown under the bands in the gel. The AuNP-to-scDNA ratio was ~100 : 1. Magnified bands of lanes 3 and 9 are shown. The ladders are in lane 6. (b) The lineout plots of another gel. The samples were prepared similarly to those in (a). Vertical lines are drawn for visual alignment of the bands.

The maximum enhancement was of the order of ~200% (three times that of the free scDNA) and occurred between 0.5 and 2 Gy of radiation dosage. The average enhancement factor was ~2.1 at 1 Gy. As high as 8 times enhancement at 0.5 Gy was observed (not shown). Further optimization is underway.

One can estimate the maximum theoretical enhancement factor by comparing the X-ray absorption cross-sections for the gold nanoparticles and water at 81 keV. Assuming that a scDNA occupies a 1.5 nm diameter cylinder, 500 nm long, and is surrounded by a 12 nm diameter cylinder of water, a distance over which Auger electrons or hydroxyl radicals are effective, the X-ray absorption cross-section for this amount of water surrounding the scDNA is 0.18 (cm^2 g^{-1}, mass absorption

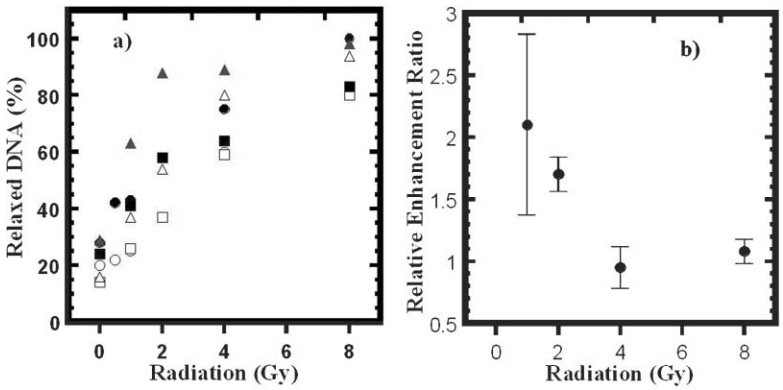

Fig. 4 Statistics of the gels on the radiation tests. The percentage of the relaxed form is plotted in (a). scDNA (empty symbols) and AuNP-scDNA (corresponding solid symbols) are shown. (b) The relative enhancement ratios as a function of radiation dosage for three sets of samples.

coefficient at 82 keV) $\times$ 1 g/cm^3 $\times$ $(6 \times 10^{-7})^2$ $\times$ π $\times$ 500 $\times$ 10^{-7} = 1.0 $\times$ 10^{-17} cm^2. The absorption cross-section for one hundred 5 nm gold nanoparticles (each contains $\sim$3300 Au atoms) decorated with the scDNA is 7.9 (cm^2 g^{-1}) $\times$ 196 amu $\times$ 900 (number of surface atoms) $\times$ 100 (number of gold nanoparticles) $\times$ 1.6 $\times$ 10^{-24} (g amu^{-1}) = 2.2 $\times$ 10^{-16} cm^2.[18] Since only half of the Auger electrons escaped from the AuNP face the scDNA, the effective absorption is half the value shown above. Therefore, 100 AuNP next to the scDNA are about 11 times as efficient as the 1.8 millions of water molecules around the scDNA.

The observed low value may be caused by the variations in the interactions between AuNP and scDNA.[19] It may also be caused by the thiol ligands (an analogue to cysteamine) that may fall off the AuNP and become radical scavengers.[4] It could also be caused by the continuum X-rays (10–100 keV) used in the experiments rather than monochromatic X-ray source at just above 81 keV used in the estimation given above.[20] Correcting these factors may further improve the potency of AuNP in cancer treatment, especially when the method is combined with other techniques such as protein drugs and polymer-based delivery vehicles.[21,22]

This work is partially supported by the NSF CAREER Award (CHE-0135132). The authors thank Professor C. F. Meares for many insightful discussions. We thank Professor A. Y. Chen at the Cancer Center at UC Davis for his kind support. We thank many colleagues and students for their experimental assistance.

Erika A. Foley, Joshua D. Carter, Fang Shan and Ting Guo*
Chemistry Department, One Shields Ave., University of California, Davis, CA 95616, USA. E-mail: tguo@ucdavis.edu; Fax: 530 752 8995; Tel: 530 754 5283

Notes and references

1 J. F. Hainfeld, D. N. Slatkin and H. M. Smilowitz, *Physics in Medicine and Biology*, 2004, **49**, N309–315.
2 M. R. McDevitt, D. S. Ma, L. T. Lai, J. Simon, P. Borchardt, R. K. Frank, K. Wu, V. Pellegrini, M. J. Curcio, M. Miederer, N. H. Bander and D. A. Scheinberg, *Science*, 2001, **294**, 1537–1540.
3 *Fighting Tumors with Gold Nanocomposites*, B. Halford, *Chem. Eng. News*, 2005, January, 29.
4 W. T. Moss and J. D. Cox, *Radiation Oncology: Rationale, Technique, Results*, 7th, The C. V. Mosby Company, St. Louis, 1994, p. 799.
5 E. J. Hall, *Radiobiology for the Radiologist*, 1st, Harper & Row, Publishers, New York, 1978, 305.
6 C. von Sonntag, *The Chemical Basis for Radiation Biology*, Taylor and Francis, London, 1987.
7 M. A. Walicka, Y. Ding, S. J. Adelstein and A. I. Kassis, *Radiation Research*, 2000, **154**, 326–330.
8 D. E. Charlton and J. A. Booz, *Radiat. Res.*, 1981, **87**, 10–23.
9 B. Boudaiffa, P. Cloutier, D. Hunting, M. A. Huels and L. Sanche, *Science*, 2000, **287**, 1658–1660.
10 D. E. Charlton and J. L. Humm, *Int. J. Radiat Biol*, 1988, **53**, 353–365.
11 R. Shenhar and V. M. Rotello, *Acc. Chem. Res.*, 2003, **36**, 549–561.
12 A. P. Alivisatos, K. P. Johnsson, X. G. Peng, T. E. Wilson, C. J. Loweth, M. P. Bruchez and P. G. Schultz, *Nature*, 1996, **382**, 609–611.
13 D. Zanchet, C. M. Micheel, W. J. Parak, D. Gerion, S. C. Williams and A. P. Alivisatos, *J. Phys. Chem. B*, 2002, **106**, 11758–11763.
14 P. Sandstrom, M. Boncheva and B. Akerman, *Langmuir*, 2003, **19**, 7537–7543.
15 J. Tien, A. Terfort and G. M. Whitesides, *Langmuir*, 1997, **13**, 5349–5355.
16 M. Brust, M. Walker, D. Bethell, D. J. Schiffrin and R. Whyman, *J. Chem. Soc., Chem. Commun.*, 1994, 801–802.
17 C. M. McIntosh, E. A. Esposito, A. K. Boal, J. M. Simard, C. T. Martin and V. M. Rotello, *J. Am. Chem. Soc.*, 2001, **123**, 7626–7629.
18 R. E. Benfield, *J. Chem. Soc.,Faraday Trans.*, 1992, **88**, 1107–1110.
19 A. Y. Chen, R. Chou, S. J. Shih, D. Lau and D. Gandara, *Crit. Rev. Oncol.-Hematol.*, 2004, **50**, 111–119.
20 D. J. Gibson, S. G. Anderson, C. P. J. Barty, S. M. Betts, R. Booth, W. J. Brown, J. K. Crane, R. R. Cross, D. N. Fittinghoff, F. V. Hartemann, J. Kuba, G. P. Le Sage, D. R. Slaughter, A. M. Tremaine, A. J. Wootton, E. P. Hartouni, P. T. Springer and J. B. Rosenzweig, *Phys. Plasmas*, 2004, **11**, 2857–2864.
21 J. A. Williams, X. Yuan, L. E. Dillehay, V. R. Shastri, H. Brem and J. R. Williams, *Int.. J. Radiat. Oncol., Biol., Phys.*, 1998, **42**, 631–639.
22 M. Mccoy, *Target Practice*, 2003, 16–17.

